advances
in radiation oncology

Scientific Article

Autoradiography and biopsy measurements of a resected hepatocellular carcinoma treated with 90 yttrium radioembolization demonstrate large absorbed dose heterogeneities

Jens Hemmingsson MS [a],*, Jonas Högberg PhD [b], Johan Mölne MD, PhD [c], Johanna Svensson MD, PhD [d], Peter Gjertsson MD, PhD [e], Magnus Rizell MD, PhD [f], Olof Henrikson MD, PhD [g], Peter Bernhardt PhD [a]

[a] *Department of Radiation Physics, The Sahlgrenska Academy, Sahlgrenska University Hospital, Gothenburg, Sweden*
[b] *Department of Medical Physics, Linköping University Hospital, Linköping, Sweden*
[c] *Department of Pathology, The Sahlgrenska Academy, Sahlgrenska University Hospital, Gothenburg, Sweden*
[d] *Department of Oncology, The Sahlgrenska Academy, Sahlgrenska University Hospital, Gothenburg, Sweden*
[e] *Department of Clinical Physiology, The Sahlgrenska Academy, Sahlgrenska University Hospital, Gothenburg, Sweden*
[f] *Department of Surgery, The Sahlgrenska Academy, Sahlgrenska University Hospital, Gothenburg, Sweden*
[g] *Department of Radiology, The Sahlgrenska Academy, Sahlgrenska University Hospital, Gothenburg, Sweden*

Abstract

Purpose: Radioembolization is an alternative palliative treatment for hepatocellular carcinoma. Here, we examine the uptake differences between tumor tissue phenotypes and present a cross-section of the absorbed dose throughout a liver tissue specimen.

Methods and materials: A patient with hepatocellular carcinoma was treated with ^{90}Y radioembolization followed by liver tissue resection. Gamma camera images and autoradiographs were collected and biopsy tissue samples were analyzed using a gamma well counter and light microscopy.

Results: An analysis of 25 punched biopsy tissue samples identified 4 tissue regions: Normal tissue, viable tumor tissue with and without infarcted areas, and tumor areas with postnecrotic scar tissue. Autoradiography and biopsy tissue sample measurements showed large dose differences between viable and postnecrotic tumor tissue (159 Gy vs 23 Gy).

Conclusions: Radioembolization of 90 yttrium with resin microspheres produces heterogeneous-absorbed dose distributions in the treatment of unifocal hepatic malignancies that could not be accurately determined with current gamma camera imaging techniques.

Introduction

Hepatocellular carcinoma (HCC) accounts for approximately 80% of primary liver cancers and is the third most common cause of cancer-related deaths worldwide.[1,2] Major risk factors for the development of HCC include hepatitis B or C infections and alcoholic liver disease. These risk factors also lead to the development of cirrhosis, which is present in 80% to 90% of patients with HCC.[3] Treatment options vary depending on the cancer stage and range from potentially curative treatments such as surgical resection, liver transplantation, or radiofrequency ablation to palliative treatments including sorafenib (tyrosine kinase inhibitor), transarterial chemoembolization, or radioembolization. During radioembolization, resin or glass microspheres that contain 90 yttrium (^{90}Y) are injected into the hepatic artery and spread throughout the injected liver, lobe, or segment, mainly reaching tumor tissue due to the predominantly arterial vascularization of liver tumors.[4] Radioembolization of ^{90}Y utilizes high-energy beta particles (E_{mean}: 0.934 MeV) and approximately 90% of the absorbed dose is delivered in the first 9 days after injection.

In 2014, Högberg et al. described the distribution of resin microspheres in the hepatic arterial tree of normal liver tissue as large clusters in arterioles or a string of spheres or single spheres in terminal arterioles.[5] This irregular arrangement leads to a heterogeneous-absorbed dose distribution that could be a contributing factor to the higher radiation tolerance that is observed in radioembolization relative to external beam radiotherapy along with the low-dose rate effects of ^{90}Y irradiation.[6] Similar estimates of tumor dose heterogeneity would be valuable to improve the evaluation of the therapeutic potential of radioembolization. Posttreatment imaging such as single photon emission computed tomography (SPECT) or positron emission tomography (PET) are important tools to evaluate activity distributions both intra- and extra-hepatic. From these images, the tumor-to-normal-tissue concentration (TNC) ratio can be calculated, which is a useful quantity in treatment planning (on pretherapeutic SPECT images) and efficacy evaluation, as follows:

$$TNC = \frac{A_T/V_T}{A_N/V_N} \qquad (1)$$

where A is the activity in tumor (T) and normal tissue (N), respectively, and V is the corresponding volume of each of these regions.

Unfortunately, the poor resolution and noise properties of gamma cameras and PET make characterization of the dose distribution in tumors challenging. SPECT imaging of ^{90}Y requires additional processing to enhance image quality since images suffer from the low photon yield and positional uncertainties of bremsstrahlung interactions as well as scattered photons and septal penetration that result from the continuous high-energy spectrum (E_{max}: 2.28 MeV) that make window-based scatter rejection difficult.[7] Compared with bremsstrahlung, SPECT and PET images show superior contrast and resolution.[8] However, the low positron-branching ratio make for long scan times and noisy images.[9]

Here, we describe and compare the estimated absorbed dose distribution in resected HCC tissue at different levels of resolution, utilizing collected gamma camera images, ex vivo autoradiography measurements, activity quantification, and pathologic analysis.

Methods and materials

Radioembolization was performed at Sahlgrenska University Hospital as a neo-adjuvant treatment to lower the risk of recurrence at the resection boundaries for a 63-year-old man with a unifocal HCC in the noncirrhotic right lobe. All procedures were approved by the regional ethics review board in Gothenburg, Sweden and were in accordance with the 1964 Helsinki declaration and its later amendments or comparable ethical standards. A total of 2.0 GBq ^{90}Y resin microspheres were injected into the right lobe, which consisted of 450 ml and 1050 ml of tumor and normal tissue, respectively. SPECT images (Infinia Hawkeye, GE Healthcare, Milwaukee, WI) were collected for the pretherapeutic simulation with 150 MBq ^{99m}Technetium-MacroAggregate Albumin (^{99m}Tc-MAA; energy window: 126-154 keV) and similarly for ^{90}Y bremsstrahlung after the radioembolization (energy window: 55-285 keV). SPECT images were reconstructed using iterative, ordered-subset, expectation maximization with computed tomography (CT)-based attenuation correction. The normal and tumor areas were outlined in volumes of interest (VOI) for SPECT quantification using hepatic, arterial, phase CT images in the imaging platform PhONSAi developed in-house (T.Rydén et al.: Fast GPU-based Monte Carlo code for SPECT/CT reconstructions generates improved 177Lu images). The TNC was calculated from the counts in the normal liver VOI and the tumor VOI. The absorbed tumor doses were calculated applying the TNC values and assuming that the

activity was retained in the liver and tumor tissue. No shunting to other organs was observed and no recovery correction was made for the limited resolution in the SPECT images.

Resection was performed 10 days after therapy. The tissue sample was fixed in buffered formaldehyde for 48 hours, sectioned into 2 mm sections, enclosed in 0.2 mm plastic film, and placed between 2 sheets of autoradiographic film (Amersham Hyperfilm MP, GE Healthcare, Milwaukee, WI). Exposure of the autoradiographic films was performed 13 to 15 days after therapy and at this time, approximately 1 Bq of ^{90}Y remained in each microsphere. To find an optimal exposure time several exposures of the films were performed. The film with the highest visually determined contrast range was selected for further analysis.

For activity quantification and tissue characterization, the central tumor slice was punched for 25 biopsy tests (0.2-0.4 cm^2) and each biopsy specimen was weighed and placed in 1 ml formaldehyde (10 %). The biopsy samples were then placed in 25 plastic vials, each with a wall thickness of 1 mm and inner diameter of 9 mm, in an automatic gamma well counter (Wizard 1480, PerkinElmer, Waltham, MA) that was previously calibrated in a suitable activity interval using a known ^{90}Y activity that was placed in the same vial and volume of formaldehyde. The resulting detector efficiency ε (0.185 counts/beta emissions) was used to calculate the mean absorbed dose to each biopsy ($\bar{D}_{biopsy}$) as follows before they were sectioned into 8 μm slices and stained with hematoxylin and eosin to enable light-microscopic analysis:

$$\bar{D}_{biopsy} = \frac{\bar{E} \cdot \frac{1}{\varepsilon} \cdot \int_0^\infty A_{0,biopsy} e^{-\lambda t} dt}{m_{biopsy}} \qquad (2)$$

where $\bar{E}$ is the mean beta particle energy of ^{90}Y that corresponds to 0.934 MeV and A_0 is the number of counts registered for each biopsy specimen counted to the time of injection.

To estimate isodose curves from the scanned autoradiograph, a saturation curve was fitted to the dose calculations of the 25 biopsies as follows:

$$f(x) = a \cdot \log(x) - b \qquad (3)$$

An R^2 value of 0.895 was obtained at values 0.71 and 0.76 for coefficients a and b, respectively. Each normalized pixel value (0.135 x 0.135 mm) was placed between 2 of 22 isodose limits and assigned to a corresponding absorbed dose between 0 Gy and 200 Gy. A threshold dose was set to 200 Gy for saturated normalized pixel values (>0.882) to account for high-activity signal saturation in the autoradiograph. Autoradiography image processing and dose calculations were performed using MATLAB R2017b software (Mathworks, Natick, MA).

An experienced pathologist classified the 25 biopsy tissue samples into 6 different morphologies: 1) Viable tumor tissue

without infarction areas, 2) viable tumor tissue with infarction areas, 3) tumor tissue with postnecrotic scar tissue, 4) normal liver tissue, 5) a mix of viable tumor and normal liver tissue, and 6) diverse tumor phenotypes types (i.e., contains ≥2 distinct areas of these classifications).

Results

Single photon emission computed tomography image evaluation

The SPECT images shown in Figure 1 illustrate the differing activity distributions between ^{99m}Tc-MAA (Figs 1A and C) and ^{90}Y (Figs 1B and D). The treatment simulation using ^{99m}Tc-MAA had a TNC of 4.4 with a coefficient of variation (CV) of 0.59 in the tumor VOI (outlined) and 0.96 in the normal tissue VOI. The mean absorbed tumor dose using ^{90}Y bremsstrahlung SPECT was 73 Gy with a TNC of 1.8. The CV was 0.35 for tumor tissue and 0.24 for normal tissue.

Autoradiograph evaluations and calculated isodose curves

The normal tissue appears as a uniform brownish area in the resected specimen (Fig 3A, left side). The microspheres are accumulated in clusters in the autoradiography and visible as small black dots with differing intensities (Fig 3B). The tumor tissue is arranged in areas of viable tumor, viable tumor with infarction, and postnecrotic scar tissue (Fig 4). Highly saturated uptakes in the tumor tissue are observed in areas with viable tumor cells and low uptake areas are associated with postnecrotic scar tissue.

The isodose curves that were calculated using the curve fit (Fig 2) demonstrate a large variation in the absorbed dose throughout the specimen (Fig 3C). The normal tissue received a mean absorbed dose of 17 Gy with a CV of 0.10 but the tumor tissue received a mean absorbed dose of 109 Gy (i.e., TNC = 6.4) and a CV of 0.27.

Activity measurement evaluation and biopsy analysis

Four tissue regions were identified in the 25 punched biopsies tissue samples after light microscopic characterization: Normal tissue, viable tumor tissue with and without infarcted areas, and tumor areas with postnecrotic scar tissue (Figs 4 and 5). Seventeen of 25 biopsies tissue samples consisted of only 1 tissue region (>90 %) and 8 biopsy tissue samples contained ≥2 regions. The results from the biopsy specimen analysis and gamma well counter are summarized in Table 1.

Table 1   Biopsy classification and absorbed dose calculations

Regions	Absorbed dose (Gy)				Mean TNC	n
	Mean	Median	Range	CV		
All HCC biopsies	121	121	9-246	0.67	5.1	21
Viable tumor without infarction areas	151	146	98-232	0.33	6.4	5
Viable tumor with infarction areas	167	188	9-246	0.50	7.0	7
Tumor with post necrotic scar tissue	23	20	13-37	0.54	1.0	3
Normal tissue	24	20	22-25	0.10	1.0	2

CV, coefficient of variance; HCC, hepatocellular carcinoma; TNC, tumor-to-normal tissue concentration ratio.
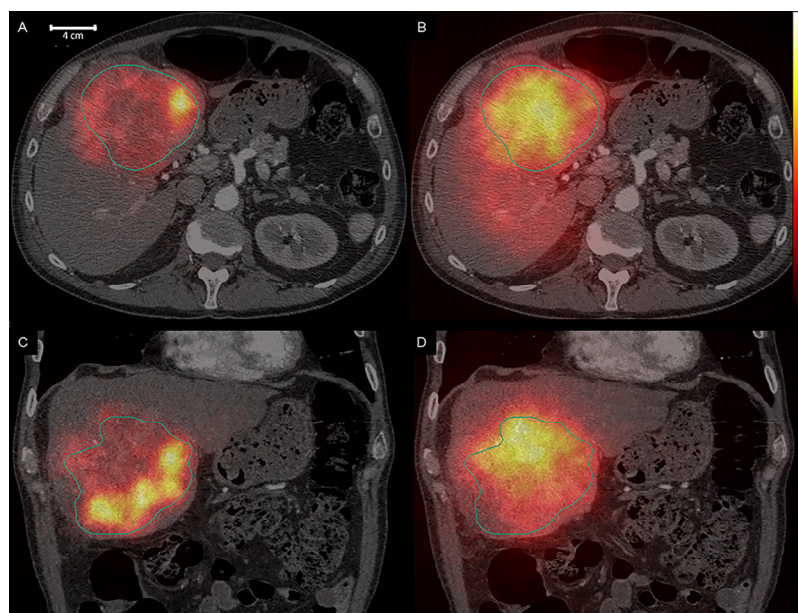
Figure 1   Transverse and coronal planes of single photon emission computed tomography/computed tomography images with the tumor volumes of interest outlined. The 99mTechnetium-MacroAggregate Albumin images in the left panels (A, C) and 90 yttrium bremsstrahlung images in the right panels (B, D).
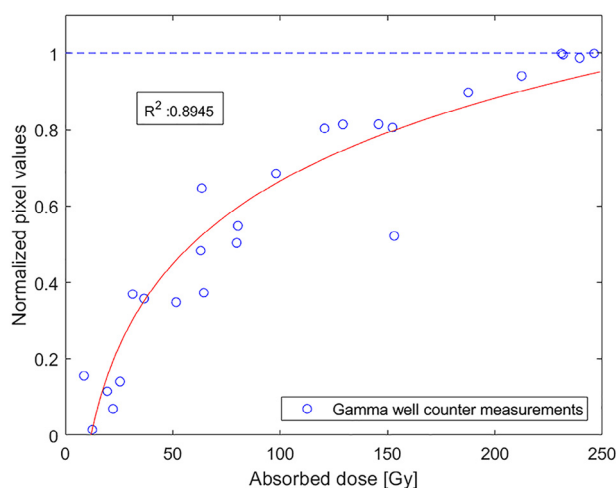
Figure 2   The saturation curve was fitted to the biopsy measurements using equation (3). Each normalized pixel value in the autoradiograph corresponds to an absorbed dose.

Discussion

Compared with the measured activity in the tumor biopsy tissue samples, the activity quantification with gamma cameras underestimates absorbed tumor doses and the heterogeneity of ^{90}Y microspheres, which are due to poor image resolution of ^{90}Y SPECT generating TNC and CV values that are too low. The biopsy specimen analysis indicated a large variation within the tumor tissue that could be partially explained by differences in tissue phenotypes.

Evaluation of the single photon emission computed tomography images

The energy spectrum along with uncertainties in the position of the emitted bremsstrahlung photon reduces the spatial resolution in SPECT images and lowers the mean absorbed dose CV and TNC. Several attempts to improve
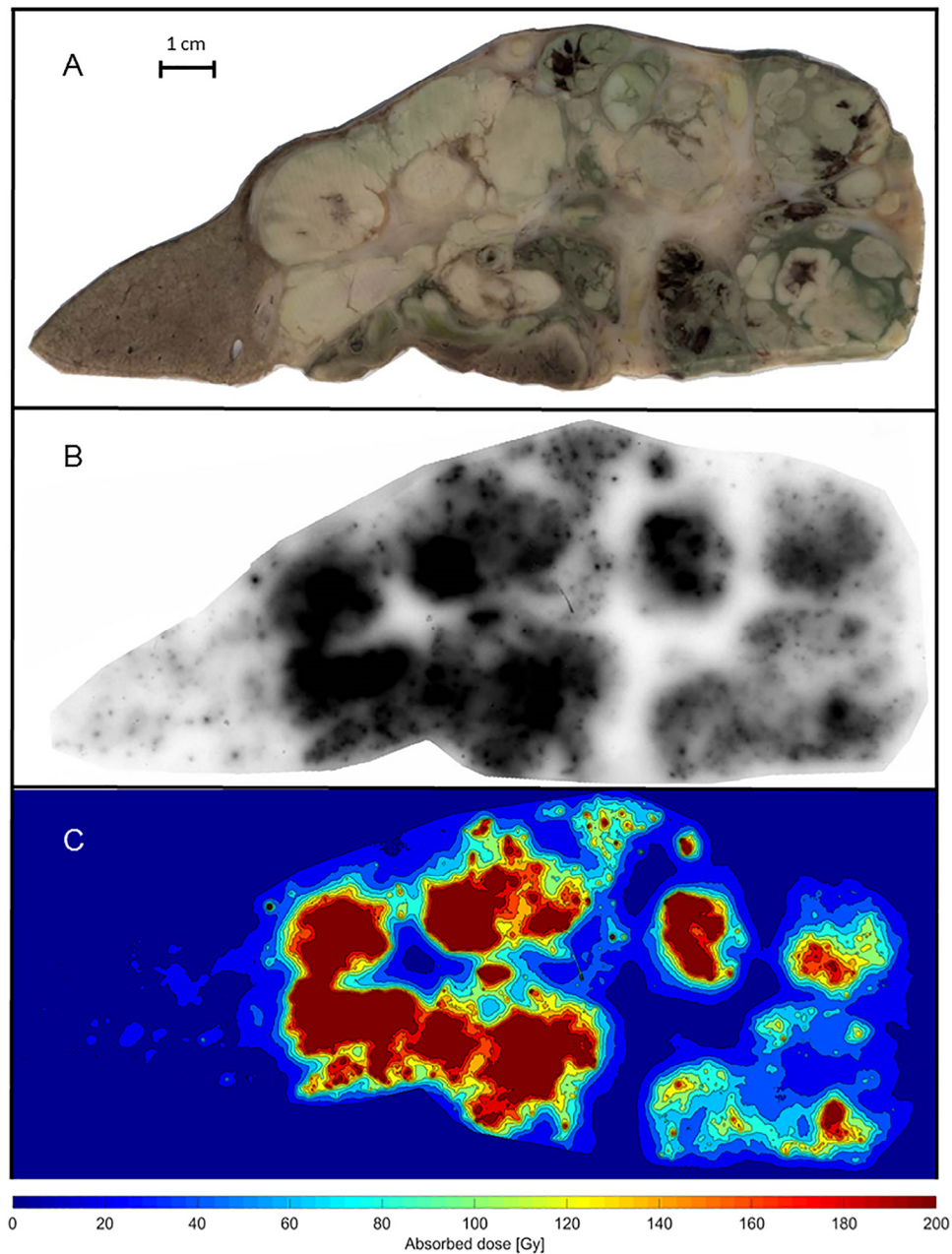
Figure 3 A-C. Photo, autoradiograph, and isodose curves (Gy) from a slice of the resected liver tissue with hepatocellular carcinoma. Normal tissue can be seen to the left in A and the maximum dose regions are depicted in black in B and dark red in C, which correspond to absorbed doses of at least 200 Gy.

image quality have been made using Monte Carlo-based SPECT reconstructions, which are necessary to accurately quantify an uptake in ^{90}Y SPECT images.[7,10] Although the average voxel value in the tumor VOI is similar for both ^{99m}Tc-MAA and ^{90}Y, the average value for the ^{90}Y in the normal tissue VOI is more than twice that seen in the MAA counterpart. However, some discrepancies between the distributions of MAA particles and microspheres are to be expected because there are differences in particle size and shape, the number of injected particles, and the time of injection.[11] Ilhan et al. reported a lack of correlation between

MAA particle distribution and resin microspheres; therefore, ^{99m}Tc-MAA might not be an optimal surrogate for detailed ^{90}Y dosimetry.[12]

Evaluation of autoradiographs and calculated isodose curves

Compared with drawing a VOI in a CT, SPECT, or PET image, the high resolution of an autoradiograph (Fig 3B) combined with resected tissue makes distinguishing between
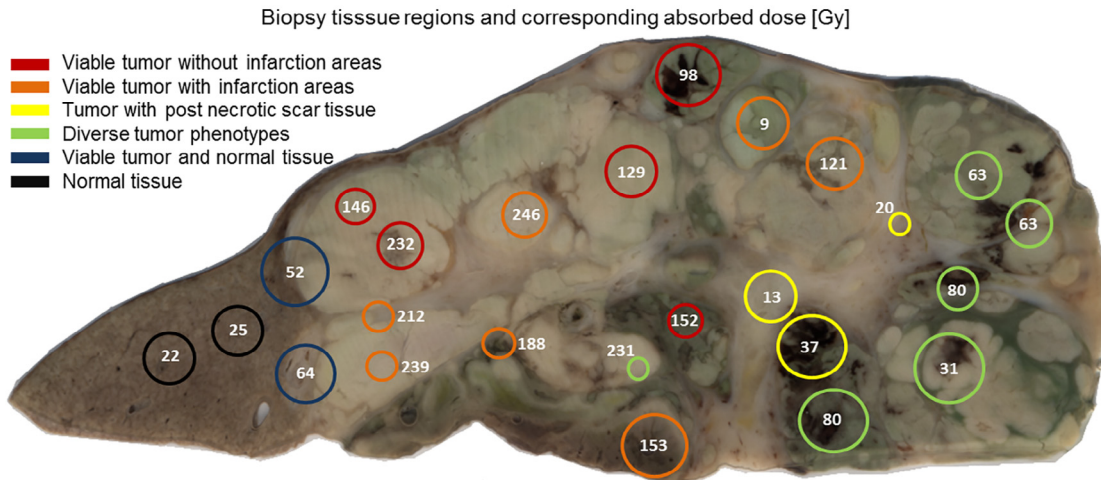
Figure 4   Results of the biopsy specimen measurements and classification with absorbed doses calculated for each biopsy tissue sample.

normal and tumor tissue relatively easy. Generally, auto-radiographs respond linearly to the logarithm of exposure in the central part of the characteristic curve[13] but deviates from this linearity for low and high exposures. This was also observed in our analysis with ^{90}Y exposure of the autoradiography.

Furthermore, in low activity regions, cross-dose effects from nearby high-activity regions cause substantial blurring since the mean range of ^{90}Y electrons in tissue is 2.5 mm. In high-activity regions, saturation affects succeeding dose calculations as mean absorbed doses may differ greatly even though exposures appear identical. For these reasons, we set the maximum absorbed dose in the saturation curve to 200 Gy, which explains the lower mean dose

calculated for the autoradiograph compared with that of the biopsy tissue samples. To conform to the gamma well counter measurements of the normal tissue, the low dose region of the curve fit (Fig 2) was not forced through the origin.

Considering these limitations, the absorbed doses seen in the isodose curves (Fig 3C) agree with previously reported tumor dose calculations.[14,15] The mean absorbed dose in normal tissue was also lower than that observed in the biopsy specimen measurements, possibly since most of these form the basis of the logarithmic saturation curve that contains HCC and the measured absorbed doses >25 Gy, which pushes the absorbed dose down for pixel values closer to zero.
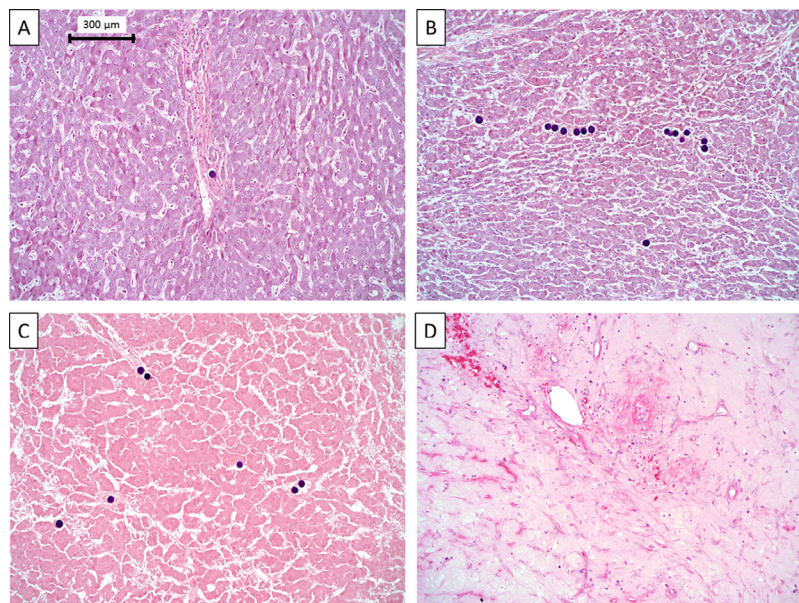
Figure 5   Tissue regions stained with hematoxylin and eosin that were found in the resected liver. Black spheres are 90 yttrium microspheres. (A) Normal liver tissue. (B-D) Viable tumor, tumor infarction, and postnecrotic scar tissue.

Autoradiography is valuable as a mean to get a detailed overview of the activity distribution. However, the invasiveness of the procedure and the sample size that is required for an adequate overview make application on a regular clinical basis problematic.

Evaluation of activity measurements and light microscopic biopsy specimen analysis

We classified the biopsy specimen phenotypes to investigate whether obvious differences in absorbed dose could be observed between tumor regions. As hypothesized, viable tumor areas are highly active and a majority (10 of 12 tumor areas) show mean absorbed doses >120 Gy, which is defined as tumoricidal.[16]

One of the viable tumor biopsy tissue samples stands out and shows an observed dose of 9 Gy, which is potentially due to a cluster formation of microspheres in the arterial tree that prevents microspheres from passing into daughter vessels beyond the cluster. This is a phenomenon that we recently described with modelling of the microspheres transport through the liver arterial tree (Högberg et al.: Simulation Model of Microsphere Distribution for Selective Internal Radiation Therapy Agrees With Observations). We demonstrated that microsphere clusters are often formed early in the arterial tree, which hampers the passage of spheres down to the final arterioles. Thereby, a highly inhomogeneous distribution of microspheres will result in some areas lacking microspheres. The simulation results agreed well with the measurements of liver tissue biopsies specimen after radioembolization. Tumor with postnecrotic scar tissue lowers the mean tumor dose, which is possibly caused by a reduced arterial circulation that reaches this region. This large-scale heterogeneity could serve as a partial explanation of the low cure rates in radioembolization.[17]

Coefficient of variation and tumor to normal tissue concentration ratio

The CV was calculated to evaluate the level of heterogeneity for all modalities in this study. The autoradiograph show microsphere heterogeneity on a geometrically relevant scale considering the beta particle range, which is in agreement with a more detailed biopsy study by Högberg et al.[5] The CV of the absorbed dose was 0.67 for all tumor biopsies and comparable results were found for the ^{99m}Tc-MAA SPECT images. A slightly lower absorbed dose CV was obtained for individual tissue phenotypes, which suggests a smaller variation within each phenotype. Smearing/cross-dose effects is an issue in both ^{90}Y bremsstrahlung SPECT images and autoradiographs and can be seen in the lower CV of approximately 0.3 of these modalities.

Assuming the mean of all tumor biopsy tissue test results provides an accurate TNC of 5.1, no other measurement modality captures the true ratio.

Conclusions

This study provides insight in the absorbed dose distribution within an HCC tumor after radioembolization using resected liver tissue. Autoradiographs and biopsies testing show the large-scale uptake heterogeneity in an HCC tumor and biopsy analysis revealed a mean absorbed tumor dose of 121 Gy with a mean absorbed dose in normal tissue of 24 Gy. The regions of viable tumor had the highest uptake but the regions with postnecrotic scar tissue showed an uptake similar to normal tissue.

Funding

References

1. Waller LP, Deshpande V, Pyrsopoulos N. Hepatocellular carcinoma: A comprehensive review. *World J Hepatol*. 2015;7:2648-2663.
2. Stewart B, Wild CP, eds. *World Cancer Report*. Geneva, Switzerland: World Health Organization; 2014:2014.
3. El-Serag HB. Hepatocellular carcinoma. *New Engl J Med*. 2011;365:1118-1127.
4. Spreafico C, Morosi C, Maccauro M, et al. Intrahepatic flow redistribution in patients treated with radioembolization. *Cardiovasc Intervent Radiol*. 2015;38:322-328.
5. Högberg J, Rizell M, Hultborn R, et al. Heterogeneity of microsphere distribution in resected liver and tumour tissue following selective intrahepatic radiotherapy. *EJNMMI Res*. 2014;4:48.
6. Pasciak AS, Bradley Y, McKinney JM, eds. *Handbook of Radioembolization: Physics, Biology, Nuclear Medicine, and Imaging*. Boca Raton, FL: CRC Press; 2016.
7. Rong X, Du Y, Ljungberg M, Rault E, Vandenberghe S, Frey EC. Development and evaluation of an improved quantitative 90Y bremsstrahlung SPECT method. *Med Phys*. 2012;39:2346-2358.
8. Elschot M, Vermolen BJ, Lam MG, de Keizer B, van den Bosch MA, de Jong HW. Quantitative comparison of PET and Bremsstrahlung SPECT for imaging the in vivo yttrium-90 microsphere distribution after liver radioembolization. *PLoS ONE*. 2013;8:e55742.
9. Pasciak AS, Bourgeois AC, McKinney JM, et al. Radioembolization and the dynamic role of 90Y PET/CT. *Front Oncol*. 2014;4:38.
10. Elschot M, Lam MG, van den Bosch MA, Viergever MA, de Jong HW. Quantitative Monte Carlo-based 90Y SPECT reconstruction. *J Nucl Med*. 2013;54:1557-1563.
11. Garin E, Rolland Y, Laffont S, Edeline J. Clinical impact of 99mTc-MAA SPECT/CT-based dosimetry in the radioembolization of liver

malignancies with 90Y-loaded microspheres. *Eur J Nucl Med Mol Imaging*. 2016;43:559-575.

12. Ilhan H, Goritschan A, Paprottka P, et al. Predictive value of 99mTc-MAA SPECT for 90Y-labeled resin microsphere distribution in radioembolization of primary and secondary hepatic tumors. *J Nucl Med*. 2015;56:1654-1660.

13. Hurter F, Driffield VC. Photochemical investigations and a new method of determination of the sensitiveness of photographic plates. *J Soc Chem Industry*. 1890;9:455-469.

14. Strigari L, Sciuto R, Rea S, et al. Efficacy and toxicity related to treatment of hepatocellular carcinoma with 90Y-SIR spheres: Radiobiologic considerations. *J Nucl Med*. 2010;51:1377-1385.

15. Gulec SA, Mesoloras G, Dezarn WA, McNeillie P, Kennedy AS. Safety and efficacy of Y-90 microsphere treatment in patients with primary and metastatic liver cancer: The tumor selectivity of the treatment as a function of tumor to liver flow ratio. *J Transl Med*. 2007;5:15.

16. Lau WY, Kennedy AS, Kim YH, et al. Patient selection and activity planning guide for selective internal radiotherapy with yttrium-90 resin microspheres. *Int J Radiat Oncol Biol Phys*. 2012;82:401-407.

17. Vilgrain V, Bouattour M, Sibert A, et al. GS-012 - SARAH: A randomised controlled trial comparing efficacy and safety of selective internal radiation therapy (with yttrium-90 microspheres) and sorafenib in patients with locally advanced hepatocellular carcinoma. *J Hepatol*. 2017;66:S85-S86.